Improving the performance of P300-based BCIs by mitigating the effects of stimuli-related evoked potentials through regularized spatial filtering

Journal of Neural Engineering

PAPER

Improving the performance of P300-based BCIs by mitigating the effects of stimuli-related evoked potentials through regularized spatial filtering

Ali Mobaien[1,*], **Reza Boostani**[1] and **Saeid Sanei**[2]

[1] Department of Electrical and Computer Engineering, Shiraz University, Shiraz, Iran
[2] School of Science and Technology, Nottingham Trent University, Nottingham NG11 8NS, United Kingdom
[*] Author to whom any correspondence should be addressed.

E-mail: ali.mobaien@gmail.com and a.mobaien@shirazu.ac.ir

Keywords: P300, brain–computer interface, visual evoked potentials, regularized xDAWN.

RECEIVED
22 February 2023

REVISED
1 January 2024

ACCEPTED FOR PUBLICATION
31 January 2024

PUBLISHED
27 February 2024

Abstract

Objective. the P300-based brain–computer interface (BCI) establishes a communication channel between the mind and a computer by translating brain signals into commands. These systems typically employ a visual oddball paradigm, where different objects (linked to specific commands) are randomly and frequently intensified. Upon observing the target object, users experience an elicitation of a P300 event-related potential in their electroencephalography (EEG). However, detecting the P300 signal can be challenging due to its very low signal-to-noise ratio (SNR), often compromised by the sequence of visual evoked potentials (VEPs) generated in the occipital regions of the brain in response to periodic visual stimuli. While various approaches have been explored to enhance the SNR of P300 signals, the impact of VEPs has been largely overlooked. The main objective of this study is to investigate how VEPs impact P300-based BCIs. Subsequently, the study aims to propose a method for EEG spatial filtering to alleviate the effect of VEPs and enhance the overall performance of these BCIs. *Approach.* our approach entails analyzing recorded EEG signals from visual P300-based BCIs through temporal, spectral, and spatial analysis techniques to identify the impact of VEPs. Subsequently, we introduce a regularized version of the xDAWN algorithm, a well-established spatial filter known for enhancing single-trial P300s. This aims to simultaneously enhance P300 signals and suppress VEPs, contributing to an improved overall signal quality. *Main results.* analyzing EEG signals shows that VEPs can significantly contaminate P300 signals, resulting in a decrease in the overall performance of P300-based BCIs. However, our proposed method for simultaneous enhancement of P300 and suppression of VEPs demonstrates improved performance in P300-based BCIs. This improvement is verified through several experiments conducted with real P300 data. *Significance.* this study focuses on the effects of VEPs on the performance of P300-based BCIs, a problem that has not been adequately addressed in previous studies. It opens up a new path for investigating these BCIs. Moreover, the proposed spatial filtering technique has the potential to further enhance the performance of these systems.

1. Introduction

The brain–computer interface (BCI) serves as a direct communication channel between the brain and a computer, allowing individuals to convey control commands through brain signals without engaging in any physical movements [1, 2]. Electroencephalography (EEG) is one of the most convenient ways to record brain activity for BCI purposes, since it is non-invasive, cheap, and widely available compared to other methods [3]. One popular type of EEG-based BCI relies on P300 signal [4], an event-related potential (ERP) that occurs as a brain response to an oddball paradigm [5]. In such paradigms, a sequence of sensory stimuli (such as visual or auditory cues) is presented, and some of

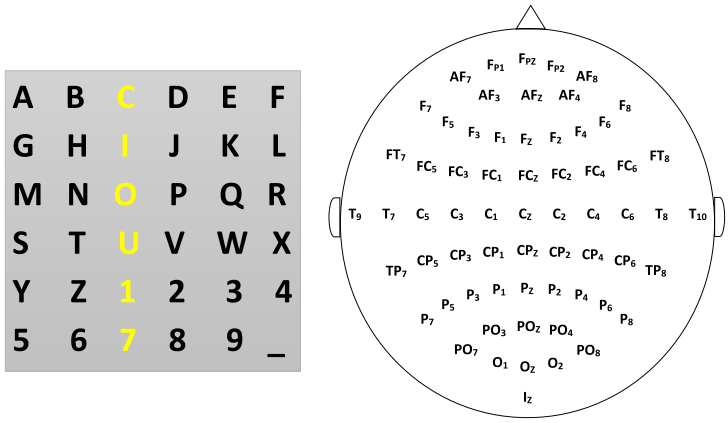

Figure 1. (a) The row-column paradigm (RCP) for spelling different characters, the third column is intensified. (b) The scalp position of the 64 electrodes used for recording P300 signals of BCI Competition III dataset.

them are rare. When the rare stimulus is detected, a positive peak in brain activity emerges approximately 300 ms later. This response can be used as a cue to control a device. A commonly used scheme in visual P300-based BCIs is an speller (VP3S) for spelling different characters based on a matrix of characters suggested by Farwell and Donchin [6], which is also known as the row-column paradigm (RCP) (figure 1(a)). In this setup, the system intensifies each row or column of the matrix at random orders. When the row or column corresponding to the desired character is intensified, the P300 signal is elicited, allowing the intended character (located at the intersection of the row and column) to be identified.

Detecting P300 from EEG signals is a complex task due to the poor signal-to-noise ratio (SNR). Despite efforts to improve the SNR, many studies have ignored the influence of visual evoked potentials (VEPs) on the P300 signal [7]. In designing RCPs or other visual P300 BCIs [4], VEPs arise together with P300 in the occipital scalp regions in response to periodic visual stimuli [7], leading to semi-periodic noise. As VEPs are present in both target and non-target data, they create confusion while classifying the trials. Any P300 can be divided into two subcomponents: p3a and p3b. The former emerges first and is closely related to attention, distributed frontally on the scalp, while the latter is related to memory update, originating from temporal-parietal scalp regions [5]. Although VEPs are predominantly observed in the occipital scalp regions, they can spread to other regions and affect P300 subcomponents.

To date, most efforts to enhance P300-based BCIs focus on improving paradigms to evoke stronger P300 signals or designing better signal processing methods [8, 9]. P300 signal processing research can be classified into two categories—P300 enhancement via filtering approaches or training more accurate classifiers.

From the first category, a common technique used in enhancing P300 is epoch averaging of the post-stimuli signals. This technique works by assuming independence between the background EEG (which has a nearly random behavior) and a well-defined P300 morphology. Through this assumption, epoch averaging cancels out the background noise, increasing the SNR [6]. However, since VEPs are time-locked to the stimuli, the averaging process may also increase their amplitudes undesirably. Another simple strategy to enhance ERP is to pass the data through a bandpass filter (BPF). ERPs have slower fluctuations compared to wide-band background EEG (0–60 Hz) [10]. Therefore, applying a BPF to raw data can improve the SNR. It's worth noting that this filtering technique does not affect VEPs as their frequency contents overlap with those of P300. Both epoch averaging and BPF are temporal filtering techniques.

Furthermore, spatial filtering methods have been widely used in the literature to enhance the P300 [11–13]. Methods such as independent component analysis (ICA) have also been employed for this purpose [14]. However, a major drawback of ICA is that it blindly separates brain signals, necessitating the involvement of an expert in manually selecting appropriate components. To address this limitation, Rivet *et al* [15] introduced an unsupervised spatial filtering method called xDAWN (the name xDAWN is driven from the final model structure specified in the original article), which aimed to identify a subspace where P300 signals were more apparent. In another study, Campos *et al* [16] developed a three-step spatial filtering method involving two principal component analysis steps, followed by ICA, to extract basic waveforms contributing to different

ERP components. It is worth noting that most studies focusing on spatial filtering also incorporate epoch averaging and BPF as preprocessing steps.

Numerous studies have attempted to integrate spatial and temporal information of P300 utilizing a cohesive spatiotemporal filtering approach. For example, Monajemi *et al* [17] devised a cooperative particle filter to track P300 parameters (e.g. amplitude, width, and latency) across successive trials. In [18], the researchers suggested a simultaneous spatiotemporal equalization procedure to whiten EEG data. This involved designing a finite impulse response filter based on a multivariate autoregressive model. They demonstrated that the whitening of EEG data can improve P300 detection in a subsequent phase. In [10], the authors formulated a P300 detection method based on temporal smoothness priors, enabling the incorporation of spatial distribution of P300 signals through a structural matrix as well. In [19], the authors proposed a modified spatiotemporal filter that extracted the data windows along both space and time dimensions to maximize the P300 SNR. They also used a discrete cosine transform-based method for artifact rejection to further improve the performance of this filter. Blanco *et al* [20] reported an improved detection rate of visual P300 spellers by introducing methods based on a selective filter bank and canonical correlation analysis, using a reduced number of trials. Lastly, Aghili *et al* [21] proposed a spatial-temporal linear feature learning approach stemmed from linear discriminant analysis (LDA) to extract high-level P300 features, in combination with discriminative restricted Boltzmann machine, for improving P300-based BCIs.

Several studies belonging to the second category attempted to design or utilize complex classifiers to detect P300 more accurately. Among these classifiers, LDA and support vector machines (SVM) have garnered more attention owing to their ease of implementation and impressive performance [4]. Some researchers have employed extensions of LDA, such as Bayesian LDA (BLDA) [22] or stepwise LDA [6], to classify P300 data, and their outcomes demonstrated improvements in the performance of VP3S systems. Other studies have utilized ensembles of LDAs and SVMs, as in [23, 24], resulting in more powerful classifiers.

Recently, there has been increasing interest in using deep neural networks (DNNs) for P300 detection. Several studies have proposed different DNN architectures for this purpose. For instance, Oralhan [25] introduced a three-dimensional convolutional neural network (3D-CNN) that achieves high accuracy in detecting P300. Zhang *et al* [26] proposed a DNN consisting of parallel spatial and temporal units for the same task. Lawhern *et al* [27] developed EEGNet, a compact CNN-based DNN that can analyze and classify brain signals from various mental activities. Additionally, there have been improved versions of EEGNet, such as the one by Zhang *et al* [28] for detecting single-trial P300 signals, as well as new DNN architectures like ST-CapsNet [29], which integrates spatial and temporal attentions using a capsule network for P300 detection, and a CNN-based approach by Du *et al* [30] that classifies single-trial P300 signals by fusing data from multiple subjects.

Among the efforts to improve visual P300-based BCIs, few have explicitly considered the impact of VEPs. In [31], authors suggested an extension of the xDAWN algorithm for enhancing error-related potentials that included a term to model both frequent and infrequent components. However, this model did not show statistically meaningful improvements for the classification of rare responses. Moreover, in [32], authors proposed a two-step statistical spatial filtering technique which showed good performance in rejecting VEPs. The first stage of this filter finds a subspace in which the Fisher criterion is maximized, and the second stage of the filter finds a subspace to maximize the SNR. The two-step final filter is a cascade of Fisher criterion and maximum SNR named C-FMS.

Contribution: in this study, we focus on VEPs and their effects on P300-based BCIs. We demonstrate that VEPs have a significant impact on P300 detection and propose a new algorithm, regularized xDAWN [15] (RxDAWN), to mitigate their effect and enhance the P300 signals simultaneously. RxDAWN addresses the P300 enhancement problem from an alternative perspective by introducing constraints to the original problem. Our study shows that RxDAWN is a general form of xDAWN and improves the performance of P300-based BCIs.

The remaining sections of this article are dedicated to exploring VEPs and their effects on visual P300-based BCIs (section 2), outlining the formulation of the RxDAWN algorithm (section 3), evaluating RxDAWN alongside xDAWN and other powerful methods using publicly available P300 datasets (section 4), discussing our findings (section 5), and concluding our study (section 6).

2. VEPs and their impact on P300-based BCIs

In this section, we aim to investigate the impact of semi-periodic VEPs on EEG recordings obtained from P300-based BCIs. To achieve this, we apply different signal analysis methods to data from an RCP dataset sourced from BCI Competition III [33]. The dataset includes recordings from two subjects (SA and SB) who spelled 185 characters (85 characters for training and 100 characters for testing). During the experiment, the subjects were presented with a 6×6 matrix of characters, with the rows and columns of the matrix randomly intensified at a frequency of

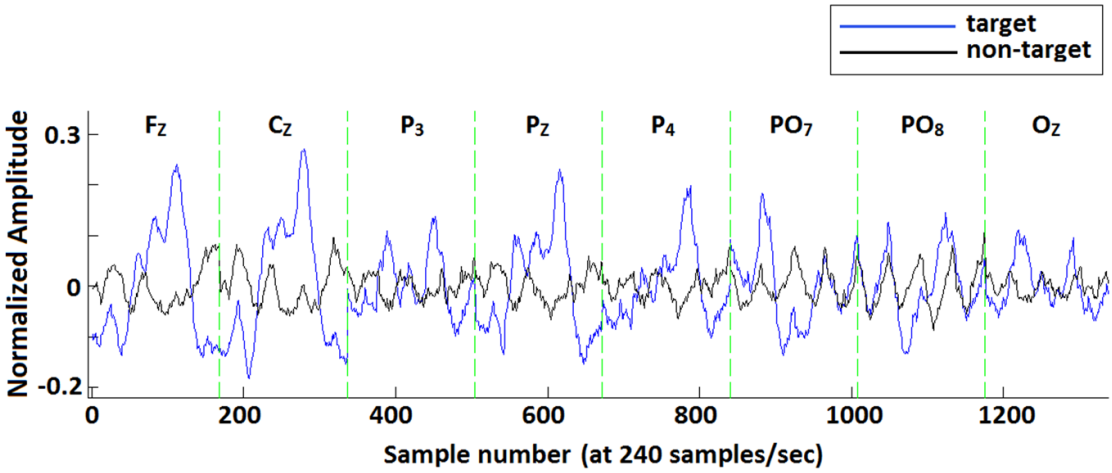

Figure 2. The average signals of target and non-target trials of SA from eight scalp electrodes (F_z, C_z, P_3, P_z, P_4, PO_7, PO_8, and O_z). They were extracted using a 700 ms window of post-stimulus signals, and the data from various channels were concatenated into a long vector. The semi-periodic VEPs are observable in both target and non-target data almost in all presented channels.

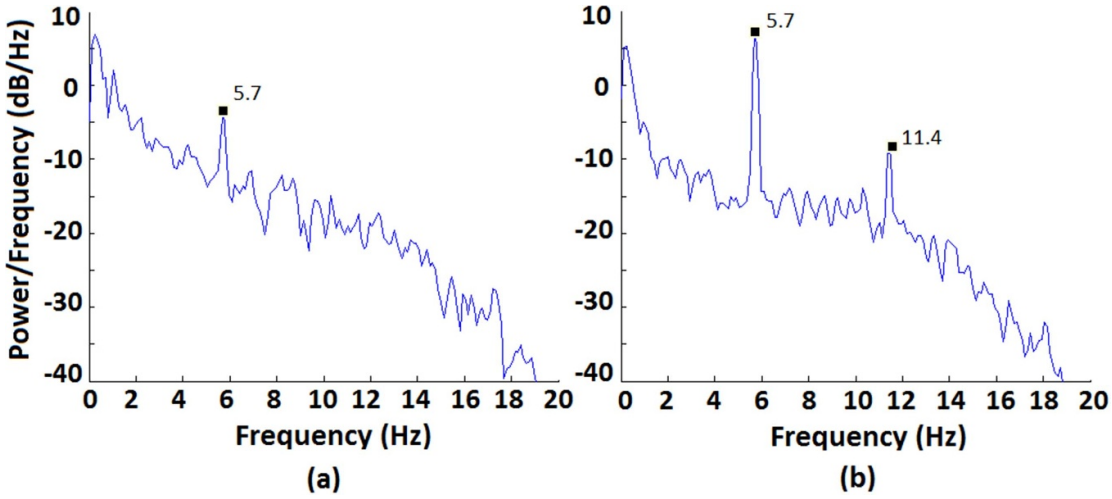

Figure 3. Power spectral density of EEG recordings (average of 85 sequences corresponding to 85 training characters) from PO_8 channel, (a) SA and (b) SB.

5.7 Hz. Each stimulus was repeated 15 times, and a total of 64 channels were used to capture the EEG signals (figure 1(b) displays a brain map showing the 64 recording electrodes). For more detailed information, refer to section 4.1.

2.1. Analysis of P300 signals and VEPs in the time and frequency domains

Figure 2 displays the average signals of multiple target and non-target trials of SA from eight scalp electrodes (F_z, C_z, P_3, P_z, P_4, PO_7, PO_8, and O_z). The signals were extracted using 700 ms windows of post-stimulus signals, and the data from various channels were concatenated into a long vector. Notably, the inter-stimulus interval (ISI) in the recording paradigm for the utilized dataset is 175 ms. The figure shows that both the target and non-target signals include a periodic component at 5.7 Hz, which is the inverse of the ISI and results from the visual stimulation (intensification of rows/columns). This component is more prominent over occipital scalp regions (PO_7 and PO_8) but also observable in the frontal regions (F_z). Figure 3 displays the power spectral density (PSD) of the EEG recordings (average of 85 sequences corresponding to 85 training characters) obtained from PO_8 channel. For SB, the second harmonic of the 5.7 Hz signal is visible at 11.4 Hz.

In figure 4, the brain energy maps in frequencies close to 5.7 Hz are displayed for both SA and SB. To create these maps, EEG signals were passed through a zero-phase BPF (a forward–backward Butterworth filter of order 4 with center frequency 5.7 Hz and bandwidth 0.3 Hz), and the average

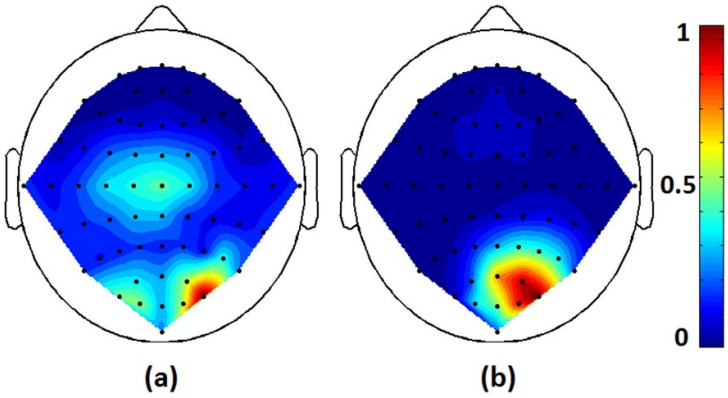

Figure 4. Energy maps of the brain for EEG activities in frequencies near 5.7 Hz for (a) SA and (b) SB.

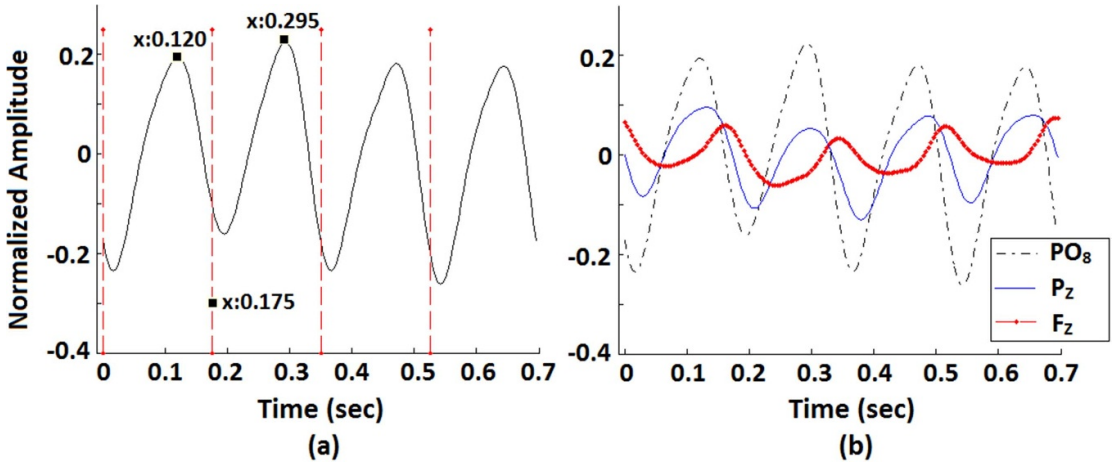

Figure 5. (a) Quasi-sinusoidal wave of four consecutive VEPs in PO_8 channel. The peaks of VEPs appear approximately 120 ms after stimuli (red lines indicate the stimuli onset). (b) VEPs originating in the occipital region (PO_8) can be propagated to other scalp regions (P_z and F_z) through conduction.

of filtered signals over the 85 training character sequences was calculated for each of the 64 recording channels. The energy of these signals was computed for each channel, normalized, and presented using brain maps. As expected, it can be seen that the energy of periodic VEPs is greatest in the visual cortex (i.e. occipital regions). Moreover, both subjects exhibit minor fluctuations in the central and frontal regions which may be related to the p3a components that occur repeatedly.

To investigate the effect of VEPs across different channels, the average of several non-target trials is plotted in figure 5. This figure is based on SB's EEG data recorded during 15 repetitions of 85 training characters. The EEG data was bandpass filtered with a range of 0.1 to 15 Hz and trials were extracted using windows of 700 ms post-stimulus signals. Figure 5(a) shows a strong semi-periodic wave consisting of four consecutive VEPs recorded from PO_8 channel. The VEP peaks appear approximately 120 ms after stimuli onset (indicated by red lines). These VEPs correspond to the P100 component, which is a positive deflection localized in the occipital region that reaches its maximum peak at around 100 ms after visual stimulus. Figure 5(b) depicts VEPs recorded from three channels (PO_8, P_z, and F_z). It is well established that the main sources contributing to VEPs are located in the occipital region of the brain [7], which is confirmed by the prominence of VEPs in PO_8 channel. Furthermore, VEPs originating in the occipital region can spread to other scalp regions (such as P_z and F_z) via volume conduction. As expected, the amplitude of VEPs decreases and their latency increases with distance from the occipital region.

2.2. P300, VEPs, and xDAWN spatial filtering

In this section, our objective is to examine the influence of VEPs on P300 enhancement using the xDAWN algorithm. XDAWN is a spatial filtering method designed to identify a subspace within the space spanned by recording electrodes where P300 signals can be enhanced [15]. The authors of [15]

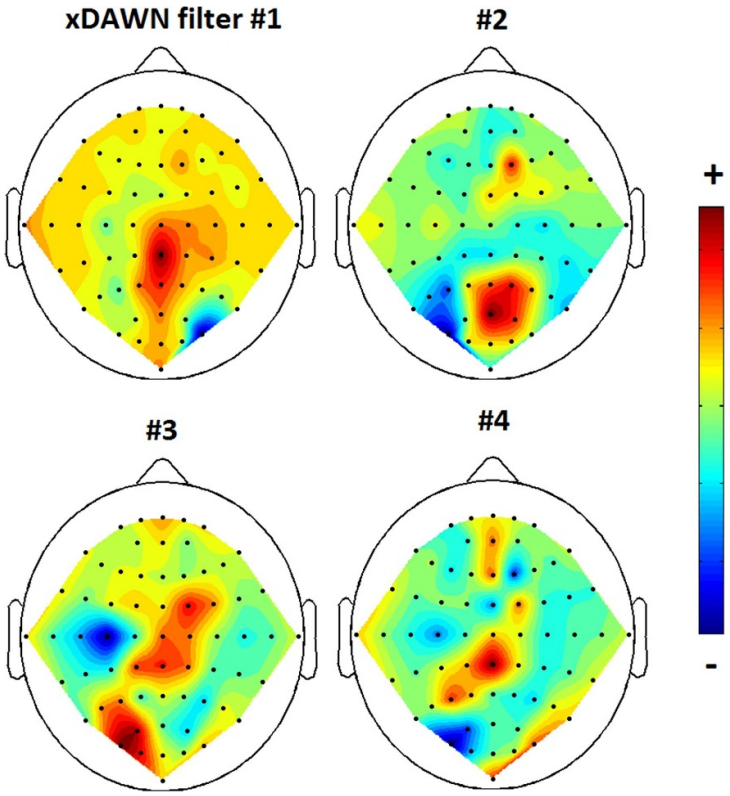

Figure 6. The brain maps indicating weight distribution of extracted xDAWN spatial filters for SB. The second filter has relatively larger VEP-related weights in the occipital region.

have explained that the first few filters contribute mostly to the P300 signals, while the later ones mainly contain noise. Therefore, it is suggested to use only the first few filters (e.g. four filters). Here, we investigate how the extracted xDAWN filters relate to VEP regions in the brain and whether the filtered signals contain any semi-periodic disturbances. To achieve this goal, we extract xDAWN filters for SB using the training set of the P300 dataset for this subject.

Figure 6 depicts the weight distribution of the first four xDAWN filters. Notably, the second filter exhibits larger VEP-related weights in the occipital region (refer to figure 4(b)). This suggests that the filtered signals produced by this filter are likely to contain stronger VEPs. To confirm this hypothesis, we performed a verification by applying the four spatial filters to filter the EEG signals and plotting their PSDs (figure 7). It is clear that the output of the second xDAWN filter exhibits the most prominent peak at 5.7 Hz.

Table 1 presents the character detection accuracies for SB test set using different xDAWN filters (see section 4.3.1 and figure 13 for the P300-based BCI block diagram). Unexpectedly, the detection accuracies when using the second xDAWN filter are much lower than those obtained using the third filter. These values should be higher for the second filter since xDAWN is designed to prioritize filtered signals with higher SNRs in the early stages. The reason for this unforseen result lies in the xDAWN's model formulation, which undesirably results in amplification of VEPs together with P300 signals.

3. Regularized xDAWN: a method to enhance P300 signals and mitigate VEPs simultaneously

As mentioned earlier, the purpose of xDAWN is to identify a spatial subspace among the electrode-covered EEG space in which P300 signals are enhanced [15]. To achieve this, xDAWN maximizes the signal variance (i.e. data containing P300) while minimizing the variance of the signal plus noise. The problem with this approach is that since target trials contain both P300 and VEPs, the spatial filters extracted by the xDAWN algorithm amplify VEPs as well. In this section, we introduce a regularized version of the xDAWN algorithm (named RxDAWN) which takes VEPs into account. This new approach allows us to add different constraints to the original problem, effectively mitigating the xDAWN's shortcoming. We demonstrate that RxDAWN represents a general form of xDAWN.

3.1. Problem formulation

Consider $X \in \mathbb{R}^{N_t \times N_s}$ as a matrix of EEG recordings obtained through the P300 evoking paradigm, where N_t is the number of temporal samples

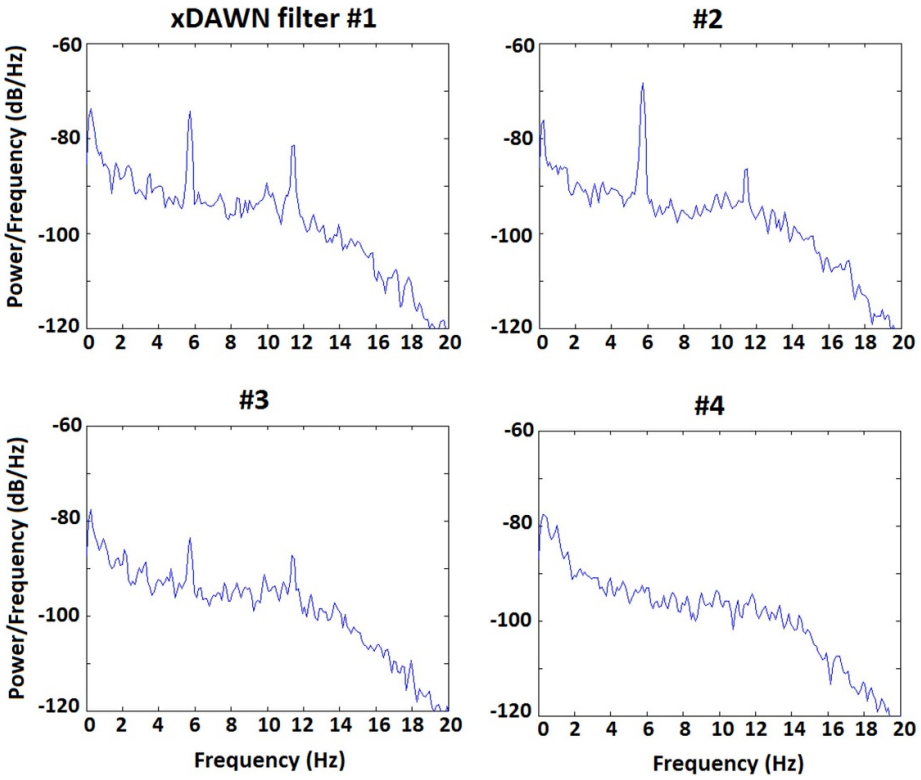

Figure 7. PSD of filtered signals by the estimated xDAWN filters for SB. The filtered signal by the second xDAWN filter has the strongest peak at 5.7 Hz.

Table 1. Accuracy percentage of character detection for P300 test set of SB using xDAWN filters for different numbers of repetitions.

	Number of Repetitions															
# xDAWN filter	1	2	3	4	5	6	7	8	9	10	11	12	13	14	15	Avg.
1st	25	37	50	56	66	70	75	74	80	86	85	88	89	89	91	70.7
2nd	6	9	9	10	14	18	19	17	21	24	20	24	25	23	22	17.4
3rd	19	31	33	41	41	43	43	52	49	57	64	70	69	72	73	50.5
4th	7	10	14	15	21	23	21	18	20	20	20	19	23	19	25	18.3
5th	5	11	7	9	8	13	14	13	14	17	17	17	20	21	24	14.0

and N_s is the number of recording electrodes. Similar to the xDAWN method, we define the data model as:

$$X = DA + N. \tag{1}$$

Here, $A \in \mathbb{R}^{N_p \times N_s}$ is a matrix containing the P300 response from various channels (electrodes), and N_p is the number of temporal samples for this response. In general, the post-stimulus window length should be sufficient to cover the entire P300 response (typically between 600 to 1000 ms). The matrix $D \in \mathbb{R}^{N_t \times N_p}$ generates duplications of A on X, wherever target stimuli are present. Based on this model, we assume that the P300 has a near-deterministic behavior after each target stimulus. The matrix D can be obtained as an asymmetric Toeplitz matrix, where its first column contains elements equal to one at the starting index of each target stimulus, and all other elements are zero. Finally, $N \in \mathbb{R}^{N_t \times N_s}$ is the noise matrix, which contains both background EEG and other disturbances (e.g. artifacts).

The objective is to determine a spatial filter $\underline{u} \in \mathbb{R}^{N_s \times 1}$ that maximizes the signal variance while minimizing the variance of the signal plus noise. We have,

$$X\underline{u} = DA\underline{u} + N\underline{u}. \tag{2}$$

Consequently, the signal-to-signal-plus-noise ratio (SSNR) is defined as:

$$\text{SSNR} = \frac{Var\{DA\underline{u}\}}{Var\{X\underline{u}\}}.$$

The spatial filter $\underline{u}$ that maximizes the SSNR can be obtained by solving the following optimization problem,

$$\hat{\underline{u}} = \arg\max_{\underline{u}} \quad Var\{DA\underline{u}\}$$
$$\text{s.t} \quad Var\{X\underline{u}\} \leqslant \delta^2. \tag{3}$$

Referring to variance as $Var\{.\}$ and using δ^2 to indicate the upper limit for the variance of signal plus noise, solving (3) requires the availability of X, D, and A; yet only the first two are readily accessible. Therefore, estimating A becomes crucial. As suggested in [15], the intuitive method for estimating A involves finding it through the least squares estimation based on the data model presented in (1). This yields,

$$\hat{A} = \left(D^T D\right)^{-1} D^T X. \tag{4}$$

However, it is necessary to note that this estimation of A remains valid only if the noise term has zero mean in each channel, otherwise, it may result in significant errors. Thus, zero-meaning the data before applying the xDAWN or RxDAWN algorithm becomes crucial. In practice, the algorithm remains unaffected since many P300-based BCIs filter (BPF) their data in the pre-processing stage and block the DC component. With zero-mean EEG data, we can estimate the variance (or power) of the desired terms via the square of their L_2-norm ($\|.\|^2$). Consequently, (3) can now be rewritten as,

$$\hat{\underline{u}} = \arg\max_{\underline{u}} \quad ||D\hat{A}\underline{u}||^2$$
$$\text{s.t} \quad ||X\underline{u}||^2 \leqslant \delta^2. \tag{5}$$

It is important to note that in (5), the normalization coefficients are discarded, having no effect on the solution.

Though solving (5) results in xDAWN filters, our objective revolves around a solution that enhances P300 signals and mitigates VEPs. Consequently, estimating $\underline{u}$ requires minimizing the variances of both noise and VEPs simultaneously. To achieve this, we represent VEPs via matrix $V \in \mathbb{R}^{N_v \times N_s}$ (N_v denotes the number of temporal samples corresponding to a selected sequence of VEPs; further details on designing V are discussed in the following paragraphs) and impose minimization of variance of $V\underline{u}$ as another constraint to (5). Both terms being positive, separate constraints are unnecessary and can be merged through summation. We also incorporate $0 \leqslant \alpha \leqslant 1$ as a balancing weight to demonstrate the effectiveness of each constraint. Thus, the SSNR for RxDAWN is defined as,

$$\text{SSNR}_{\text{RxDAWN}} = \frac{Var\{DA\underline{u}\}}{(1-\alpha)\,Var\{X\underline{u}\} + \alpha Var\{V\underline{u}\}}$$

and the optimization problem for RxDAWN takes the following form,

$$\hat{\underline{u}} = \arg\max_{\underline{u}} \quad ||D\hat{A}\underline{u}||^2$$
$$\text{s.t} \quad (1-\alpha)\,||X\underline{u}||^2 + \alpha||V\underline{u}||^2 \leqslant \delta'^2 \tag{6}$$

where δ'^2 is an upper limit for the updated constraint. Equation (6) can be converted into an unconstrained problem using a Lagrange multiplier λ,

$$L(\underline{u}) = \underline{u}^T \hat{A}^T D^T D \hat{A}\underline{u} - \lambda\left((1-\alpha)\,\underline{u}^T X^T X\underline{u} + \alpha \underline{u}^T V^T V u\right) \tag{7}$$

and $\lambda \geqslant 0$. To solve this problem we should find $\underline{u}$ so that $\partial L(\underline{u})/\partial \underline{u} = 0$. By defining $C_x \in \mathbb{R}^{N_s \times N_s} \triangleq X^T X$, $C_v \in \mathbb{R}^{N_s \times N_s} \triangleq V^T V$, and $\Psi \in \mathbb{R}^{N_s \times N_s} \triangleq X^T D(D^T D)^{-1} D^T X$, we have,

$$L(\underline{u}) = \underline{u}^T \Psi^T \underline{u} - \lambda \underline{u}^T\left[(1-\alpha)\,C_x + \alpha C_v\right]\underline{u}. \tag{8}$$

Therefore,

$$\frac{\partial L(\underline{u})}{\partial \underline{u}} = 2\underline{u}^T \Psi^T - 2\lambda \underline{u}^T\left((1-\alpha)\,C_x + \alpha C_v\right) = 0 \tag{9}$$

$$\Rightarrow \Psi\,\underline{u} = \lambda\left((1-\alpha)\,C_x + \alpha C_v\right)\underline{u} \tag{10}$$

$$\Rightarrow \left((1-\alpha)\,C_x + \alpha C_v\right)^{-1}\Psi\,\underline{u} = \lambda\underline{u}. \tag{11}$$

Based on (11), the spatial filter that maximizes (6) is obtained through eigenvalue decomposition of $C \in \mathbb{R}^{N_s \times N_s} \triangleq ((1-\alpha)C_x + \alpha C_v)^{-1}\Psi$, and $\hat{\underline{u}}$ is the eigenvector corresponding to the largest eigenvalue. The full set of spatial filters can be obtained by $C = U\Lambda U^T$, where $\Lambda \in \mathbb{R}^{N_s \times N_s}$ is a diagonal matrix of eigenvalues and the columns of $U \in \mathbb{R}^{N_s \times N_s}$ are the eigenvectors. By sorting the eigenvalues in descending order, the first corresponding eigenvectors are used to reconstruct the signal while the last ones belong to noise. It is important to note that using only one spatial filter (or basis) is not enough to fully span the signal subspace. N_f, the optimal number of eigenvectors constituting the signal subspace, should be found through experiments. In the original xDAWN article, it is suggested to use the few first filters (e.g. $N_f = 4$).

To obtain the projection of $\hat{A}$ onto the bases of enhanced subspace, we can use,

$$\hat{\underline{a}}^{(i)}_{\text{enhanced}} = \hat{A}\hat{\underline{u}}_i = \left(D^T D\right)^{-1} D^T X \hat{\underline{u}}_i \tag{12}$$

where $\hat{\underline{u}}_i$ represents the ith eigenvector of C ($i = 1, 2, \ldots, N_f$).

Comparing (5) with (6), it becomes clear that RxDAWN can be viewed as a general form of xDAWN algorithm; in fact, by letting $\alpha = 0$, the two are the same. Increasing α penalizes VEPs more, yielding spatial filters that mitigate VEPs fluctuations to a greater extent.

3.2. Encoding VEPs

C_v represents the spatial covariance of VEPs, and various methods can be employed to estimate it. For instance, V can be obtained by passing each channel of EEG recordings (X) through a narrow BPF around the VEPs frequency (e.g. 5.7 Hz in the case of P300 data from BCI Competition III), and then $C_v = V^T V$. The spatial covariance of VEPs can also be obtained after data segmentation. Consider $X_{nt}^k \in \mathbb{R}^{N_{tr} \times N_s}$ ($k = 1, 2, \ldots, K_{nt}$) as the k'th non-target trial passed through the mentioned narrow BPF (N_{tr} is the number of temporal samples within each trial, and K_{nt} is the total number of non-target trials). Then, we could concatenate the non-target trials in matrix V so that $V^T \in \mathbb{R}^{N_s \times (K_{nt} \times N_{tr})} = [(X_{nt}^1)^T, (X_{nt}^2)^T, \ldots, (X_{nt}^{K_{nt}})^T]$, and again $C_v = V^T V$.

Alternatively, we can consider C_v as a penalty matrix to penalize electrodes (recording channels) that are primarily linked to VEPs when calculating spatial filters. In this case, C_v is defined as a diagonal matrix with diagonal elements indicating the penalties. These penalties can be determined based on the energy of VEPs in each channel (e.g. the energy of signals in each channel after a narrow BPF around the VEPs frequency). To do this, it is enough to calculate $C_v = V^T V$ as described above, and then set the off-diagonal elements of C_v to zero. The penalties can also be set based on the available knowledge about the VEPs related and unrelated channels in neurophysiology.

4. Evaluation of the RxDAWN algorithm

4.1. Data

To evaluate the performance of RxDAWN, we utilized four publicly available visual P300 datasets, each described below.

4.1.1. Dataset 1: BCI Competition III-II

Dataset II of BCI Competition III [33] comprises data collected from two subjects (SA and SB) while spelling 185 characters (85 for training and 100 for testing). Subjects were presented with a 6×6 matrix of characters and instructed to focus on the desired character (as shown in figure 1(a)). The matrix's rows and columns were randomly intensified at a rate of 5.7 Hz (illuminated for 100 ms, followed by a blank matrix for 75 ms), with two of the twelve intensifications containing the desired character. Each stimulus was repeated 15 times, and EEG signals were captured using 64 channels. The signals were filtered with a 0.1 to 60 Hz BPF and digitized at 240 Hz (figure 1(b) displays a brain map of the 64 recording electrodes).

4.1.2. Dataset 2: BNCI Horizon 2020

The brain/neural computer interaction (BNCI) Horizon 2020 dataset [34] includes data from eight subjects tasked with spelling ten characters using a similar RCP paradigm as in the first dataset. The differences include a rate of 6.25 Hz for the intensification of rows and columns and the use of only eight channels (F_z, C_z, P_3, P_z, P_4, PO_7, PO_8, and O_z) to capture EEG signals.

4.1.3. Dataset 3: BCIAUT-P300

The BCIAUT-P300 dataset [35] involves fifteen subjects attempting to identify eight objects in a virtual environment. Each block consists of the user trying to identify one of the eight objects as the target. For each block, k_r runs are repeated, with each run composed of a single flash of each object presented for 100 ms at different times and in random order, with an ISI of 200 ms (i.e. a flash rate of 5 Hz).

Participants underwent seven identical training sessions on different days. The data recorded from each session is divided into two parts: training and test data. The training data consists of 20 blocks, each containing 10 runs. Considering eight objects, this results in $20 \times 10 \times 1$ target P300 signals and $20 \times 10 \times 7$ non-target signals. In contrast, the test data consists of 50 blocks for each participant, using 3 to 10 runs per block.

EEG data were recorded from 8 active electrodes positioned at C_3, C_z, C_4, CP_z, P_3, P_z, P_4, and PO_z locations. The sampling rate was 250 Hz, and the data were processed through a 50 Hz notch filter and then band-pass filtered between 2 and 30 Hz.

4.1.4. Dataset 4: RSVP

The final dataset used in this study is a single-trial P300 dataset from a rapid serial visual presentation (RSVP) paradigm [36]. Collected from 64 subjects divided into two groups (A and B), each participant was instructed to identify their desired image while maintaining covert attention without moving their eyes. Each group contained two blocks, with 40 trials in each block and 100 images presented in each trial. EEG signals were recorded using 64 channels at a sampling rate of 240 Hz.

4.2. Suppressing VEPs and enhancing P300 signals by RxDAWN filters

In this study, we aim to investigate the efficacy of RxDAWN filters in suppressing VEPs after spatial filtering of EEG data. To accomplish this, we obtain C_v as the spatial covariance matrix of non-target trials and extract RxDAWN filters for different values of α, including $\alpha = 0$, $\alpha = 0.25$, $\alpha = 0.5$, and $\alpha = 1$.

Brain maps illustrating the weight distribution of the first four extracted RxDAWN filters for SB from the BCI Competition III-II dataset are presented in figure 8, while figure 9 displays the PSD of filtered signals by these filters. When $\alpha = 0$, RxDAWN filters have significant VEP-related weights in the occipital region (refer to figure 4(b)), particularly in the second filter, resulting in strong peaks at 5.7 Hz and 11.4 Hz

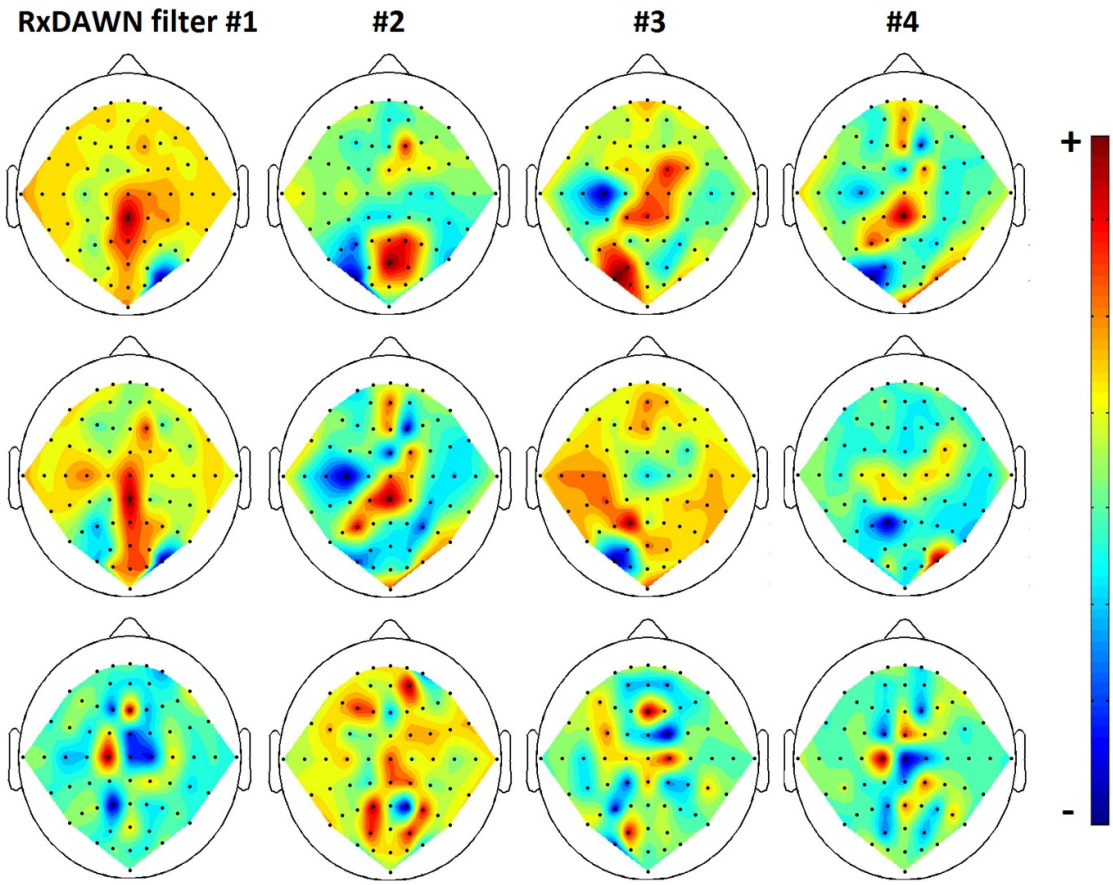

Figure 8. The brain maps indicating the weight distribution of extracted RxDAWN filters for SB. The first row depicts the extracted filters for $\alpha = 0$, the second row depicts the extracted filters for $\alpha = 0.5$, and the third row depicts the extracted filters for $\alpha = 1$.

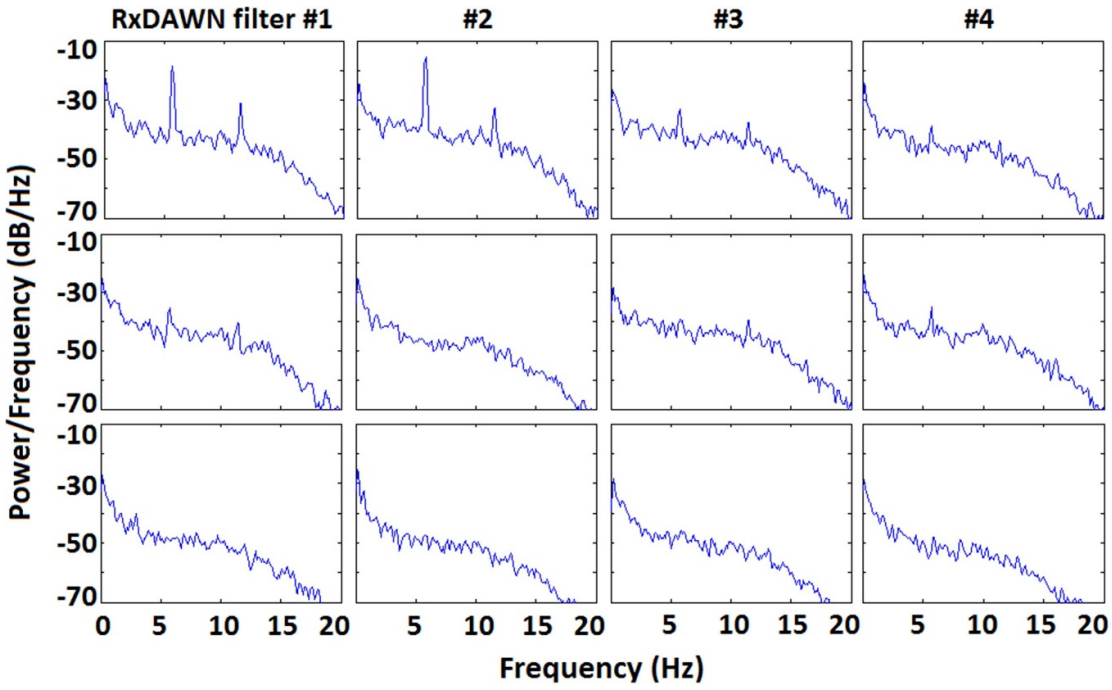

Figure 9. PSD of the filtered signals using the extracted RxDAWN filters for SB. The first row corresponds to the extracted filters for $\alpha = 0$, the second row corresponds to the extracted filters for $\alpha = 0.5$, and the third row corresponds to the extracted filters for $\alpha = 1$.

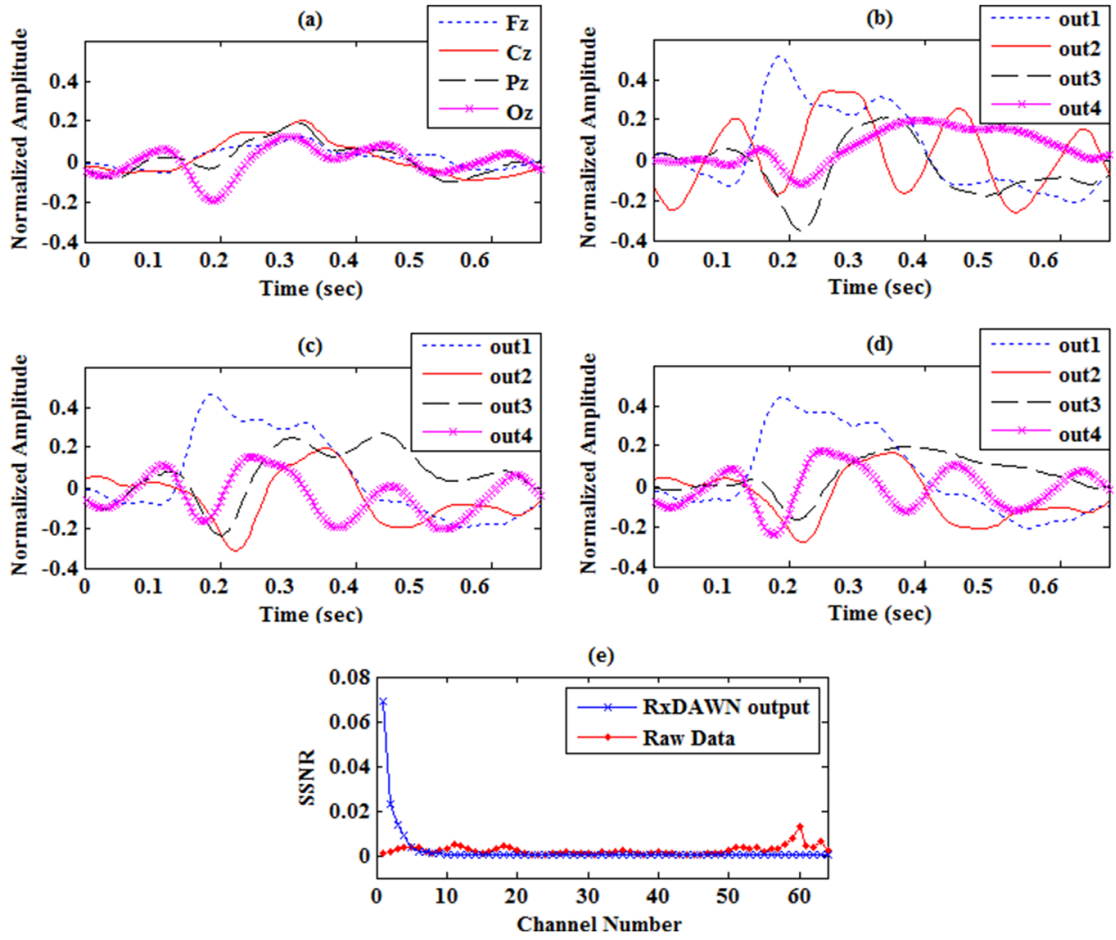

Figure 10. The estimated P300 signals and SSNR of data before and after RxDAWN spatial filtering.
(a) Estimated P300 in four channels (F_z, C_z, P_z, and O_z) before spatial filtering. (b)–(d) Estimated P300 after spatial filtering with α equal to 0, 0.25, and 0.5, respectively. (e) SSNR of each channel of EEG data before and after filtering.

in the PSD of filtered signals. This outcome can be explained by the fact that for $\alpha = 0$, RxDAWN attempts to identify a subspace where the power of the signal is amplified while simultaneously reducing the power of the signal plus noise. Since VEPs exist in both signal and noise components, they are also amplified. By increasing α to 0.5, the weight distribution is modified to reduce the power of VEPs, as evidenced by the decreased weights in the occipital regions in the second filter. As expected, this leads to a reduction in the PSD of filtered signals at 5.7 Hz and 11.4 Hz. When $\alpha = 1$, RxDAWN is biased towards suppressing only VEPs. As can be seen, the weights are arranged with opposite signs in nearby electrodes. For instance, in the second filter, the midline negative weights in the occipital region are surrounded by positive weights. This is because VEPs emerge with similar phase and amplitude in nearby electrodes, but their phases and amplitudes differ in distant electrodes, as shown in figure 5.

It is important to note that while setting $\alpha = 1$ effectively removes VEPs, other sources of noise are not taken into account, potentially leading to a decline in RxDAWN's performance. As a result, determining the optimal α value that balances the suppression of VEPs and other sources of noise should be accomplished through cross-validation during the training phase of RxDAWN.

Figure 10 displays the estimated P300 signals and SSNR of data before and after RxDAWN spatial filtering (data from SB of the BCI Competition III-II dataset). Figure 10(a) represents the estimated P300 in four channels (F_z, C_z, P_z, and O_z) using (4), while figures 10(b)–(d) represent the estimated P300 after spatial filtering by the first four RxDAWN filters using (12). Additionally, α is set to 0, 0.25, and 0.5 for figures 10(b)–(d), respectively. P300 amplitude is significantly improved in RxDAWN outputs. When $\alpha = 0$, the output of the second filter shows a strong semi-sinusoid activity related to VEPs. However, by increasing α, this component is suppressed in the first filters and shifted to RxDAWN channels with lower energy. Figure 10(e) shows the SSNR of each channel of EEG data before and after filtering, indicating a significant improvement in SSNR in the first few RxDAWN channels.

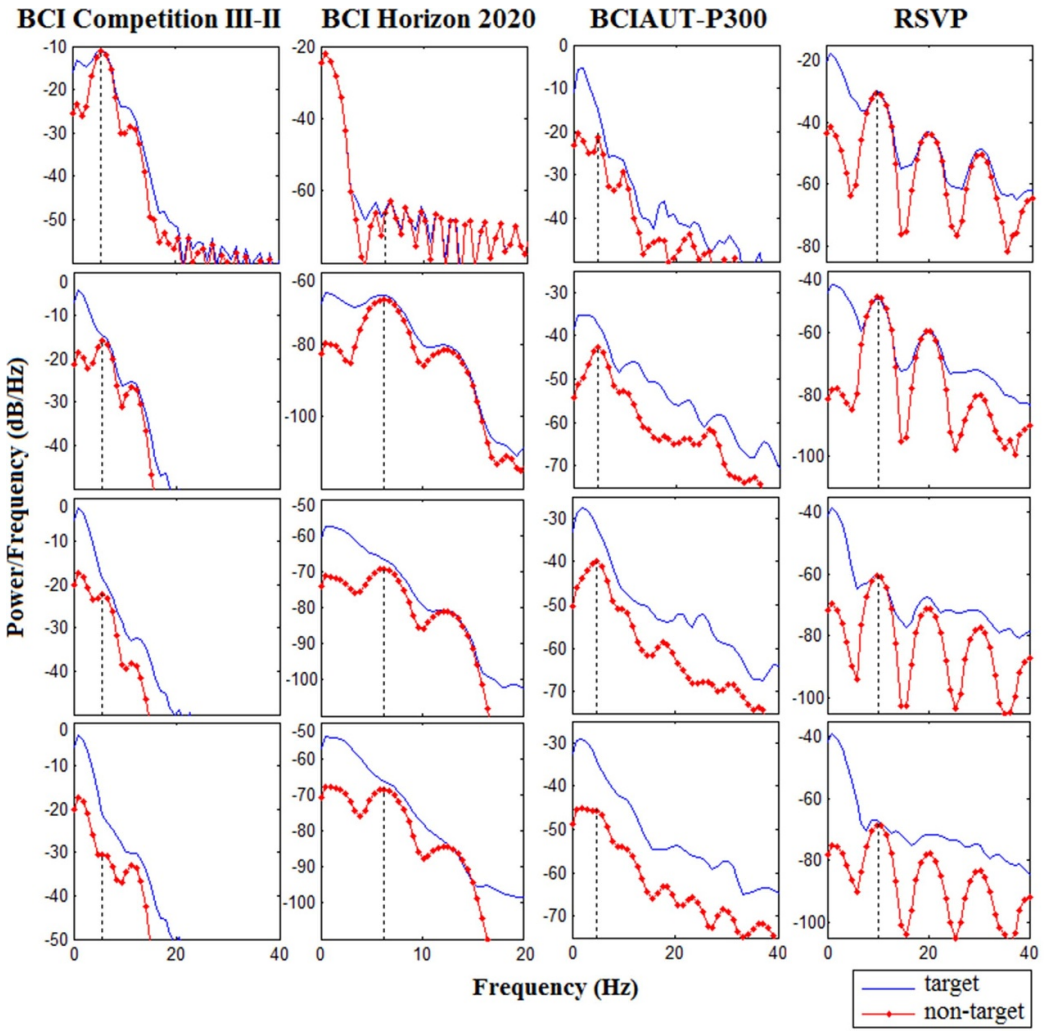

Figure 11. The PSD of the average of all target and non-target trials across all subjects within each dataset. First row from above: raw data from occipital region channels. Second row: first output of xDAWN or RxDAWN with $\alpha = 0$. Third row: First output of RxDAWN with $\alpha = 0.25$. Fourth row: first output of RxDAWN with $\alpha = 0.50$.

To assess the impact of VEPs in different datasets used in this study, figure 11 is presented. In the first row from above, the PSD of the average of all target and non-target trials across all subjects within each dataset from occipital region channels (PO_z for the BCIAUT-P300 dataset and PO_8 for others) are plotted. The black dashed line marks the frequency of visual stimuli. Across all plots, the PSD of target and non-target data in the frequency of visual stimuli either overlap or are very close. For datasets 1 and 4 (i.e. BCI Competition III-II and RSVP), VEPs result in strong peaks in the PSD of EEG signals. Although VEP peaks are not as strong in datasets 2 and 3 (i.e. BNCI 2020 and BCIAUT-P300), they are still observable.

The subsequent rows in figure 11 display the PSD of average signals after spatial filtering (second row: xDAWN or RxDAWN with $\alpha = 0$, third row: RxDAWN with $\alpha = 0.25$, and fourth row: RxDAWN with $\alpha = 0.50$). Generally, RxDAWN with $\alpha = 0$ fails to mitigate the effect of VEPs. In fact, for the BNCI Horizon 2020 and BCIAUT-P300 datasets, VEPs are amplified when $\alpha = 0$. This is because both target and non-target data contain VEPs, and conventional xDAWN or RxDAWN with $\alpha = 0$ undesirably amplifies VEPs together with P300 signals (see section 3 for more explanation). However, by increasing α from zero, VEPs are attenuated, and the PSD difference between target and non-target data in stimulus frequency increases.

For a comparison between RxDAWN and other spatial filters rather than xDAWN, figure 12 displays the PSD of average signals after spatial filtering using C-FMS. Again, the first row from above depicts the PSD of averaged trials from occipital region channels. The second row depicts the PSD of averaged signals from the first-stage output of C-FMS, and the third row depicts the PSD of averaged signals from the second-stage output of this method. As observed, C-FMS first-stage filter can attenuate VEPs to some

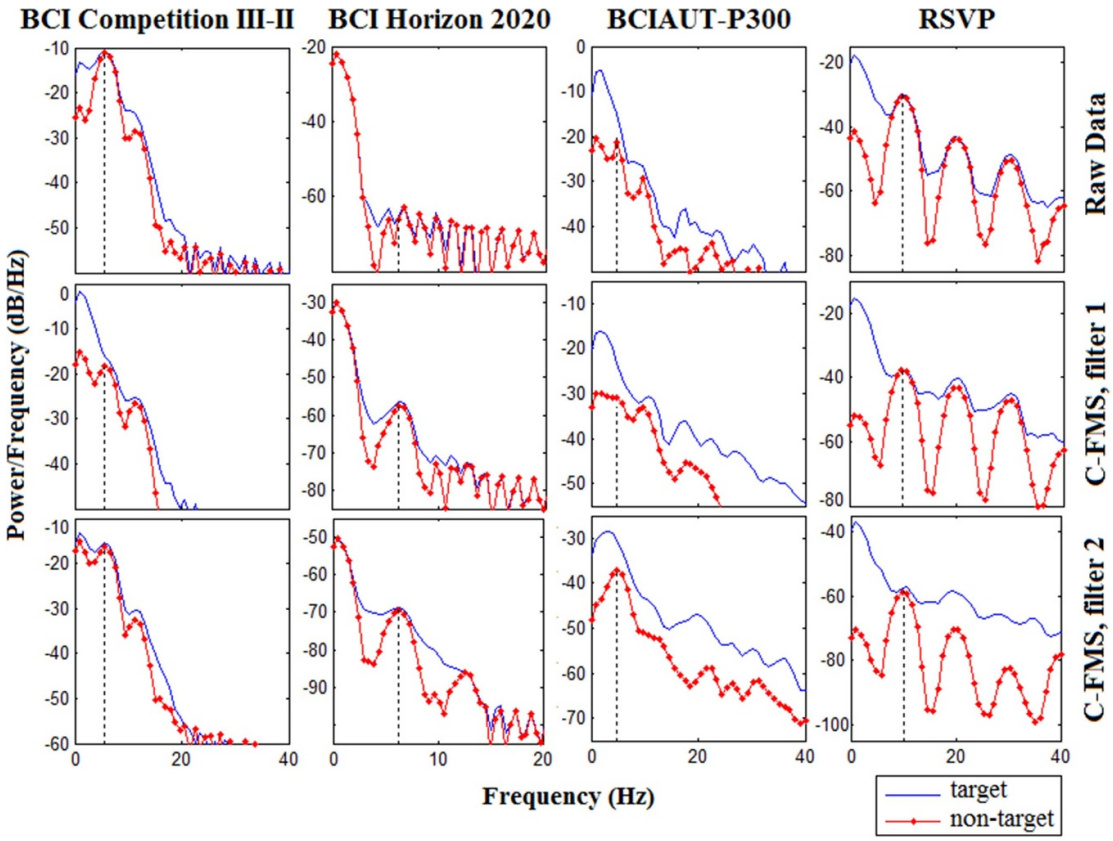

Figure 12. The PSD of the average of all target and non-target trials across all subjects within each dataset. First row from above: raw data from occipital region channels. Second row: first stage output of C-FMS. Third row: second stage output of C-FMS.

extent. However, RxDAWN outperforms C-FMS in VEPs attenuation. The second stage of C-FMS does not show VEP attenuation. The difference in performance between the first and second stages of C-FMS filtering arises from the fact that in the first stage, C-FMS aims to maximize the ratio of the between-class scatter matrix to the within-class scatter matrix. Since VEPs are attenuated in the between-class scatter matrix and exist in the within-class scatter matrix, the first stage can mitigate VEPs. However, the second-stage filter aims to maximize the ratio of the target-class covariance matrix to the non-target-class covariance matrix. Here, since VEPs are presented in both target and non-target covariance matrices, the second filter fails to mitigate VEPs.

4.3. Character, object, and P300 detection using RxDAWN method

The ultimate objective of a P300-based BCI is to accurately detect different characters (objects) spelled (selected) by a user. This task is more complex than solely identifying P300 signals. For instance, in the first two datasets (i.e. BCI Competition III-II and BNCI Horizon 2020), which are based on RCP, the chance level for correct character detection is 1/36. For the BCIAUT-P300 dataset, the chance level for correct object detection is 1/8. However, the chance level for correct P300 detection (i.e. deciding whether a trial contains P300 or not) in balanced datasets is 1/2. Here, we evaluate the performance of RxDAWN using the four described datasets for both character (object) and P300 detection.

In addition to RxDAWN, five other methods have been implemented, and RxDAWN's performance is compared to theirs. These methods are xDAWN, C-FMS, C-FMS*, BLDA, and SVM. C-FMS* is a variant of C-FMS in which the number of spatial filters used is increased while a performance improvement is observed (with a maximum of eight filters). Since the results indicated that using only two spatial filters is not sufficient to fully span the signal subspace, this modification is applied to C-FMS, significantly enhancing its performance.

The signals processed through spatial filters (i.e. RxDAWN, xDAWN, C-FMS, and C-FMS*) are fed to a BLDA for final class prediction. However, unprocessed data is fed to BLDA and SVM for classification. For SVM, the least square method is employed as its optimization technique, and a linear function is used as its kernel.

In addition to the five mentioned methods, some of the results are also compared to the outcomes of several powerful deep structures from the literature, as explained in section 4.3.3.

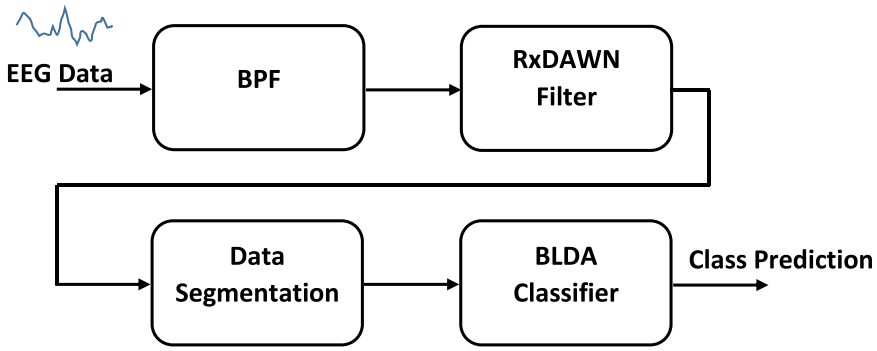

Figure 13. P300-based BCI block diagram.

4.3.1. Components of the RxDAWN-based BCI

In figure 13, an end-to-end block diagram of the proposed BCI is presented, with RxDAWN serving as one of its core units. The raw EEG data is initially passed through a BPF (a 0.1 to 15 Hz Butterworth filter of order 4 for the first two datasets and a 0.5 to 40 Hz Butterworth filter of order 4 for the fourth dataset, the third dataset was already filtered between 2 to 30 Hz). The filtered data is then fed to RxDAWN to enhance P300 and mitigate VEPs. The third step involves segmenting the filtered data and extracting post-stimuli trials using 1000 ms windows. The data is down-sampled by 4 (and for RCP datasets, normalized to have zero mean and unit variance in each channel), with the data from different channels concatenated into a long vector for each trial. A BLDA classifier is then applied to find the label (target or non-target) for each trial [22].

4.3.2. Statistical tests

Prior to testing, the P300-based BCIs must undergo training using the training data. This is done separately for each subject. While for both SA and SB from the BCI Competition III-II dataset, the training and test sets are chosen as described in the dataset documentation (see section 4.1), for the subjects of BNCI Horizon 2020 dataset a 10-fold cross-validation approach is adopted due to the limited number of spelled characters by each participant. Then, the average results of the 10 folds are reported. The training and test data for each subject and each session of the BCIAUT-P300 dataset are also chosen as described in the dataset documentation. For each subject of the RSVP dataset, the data from the first block is used for training, and the data from the second block is used for testing.

In the RxDAWN training phase, C_v is obtained based on the energy of VEPs in each channel and is used to penalize VEPs-related channels (see section 3.2). The optimal value of α is determined through cross-validation on the training set by varying α from 0 to 1. For subjects from the BNCI Horizon 2020 dataset, a nine-fold cross-validation is used, while for the other subjects from other datasets, a ten-fold cross-validation is employed. The classification results for each fold at different α values are calculated, and the average results across all those folds are used to determine the optimal α value. To make the search simpler, it is suggested to normalize C_x and C_v so that they are in the same scale (for example, by dividing their elements to the maximum value of their diagonal elements). For instance, we have found $\alpha = 0.25$ and $\alpha = 0.05$ to be suitable values for SA and SB from the BCI Competition III-II dataset, respectively. Note that after extracting spatial filters using RxDAWN, the first three to seven filters are used to filter the data. This reduces the number of channels to a minimum of 3 or a maximum of 7 channels. Although these settings have yielded good results, they can be slightly adjusted based on user preference and application requirements.

During the training phase of both BLDA and SVM, the classifiers are provided with independent sets of target and non-target trials for each repetition. These classifiers assign higher scores to target data and lower scores to non-target data. In the test phase using RCP datasets (i.e. BCI Competition III-II and BNCI Horizon 2020), the score is computed for different rows and columns of each character. The character prediction is based on the intersection of the row and column with the highest scores. To improve the P300 SNR, the trials corresponding to each row or column are averaged over a range of repetitions ($k_r = 1, 2, \ldots, 15$) in chronological order. For BCIAUT-P300 data, in each block, the object with the highest score is identified as the target. To improve the P300 SNR, the trials corresponding to each object are averaged over a range of repetitions ($k_r = 1, 2, \ldots, 10$) in chronological order. In certain test data within the BCIAUT-P300 dataset, the number of repetitions is less than 10. To maintain consistency in reported results, in such cases, the maximum result available for a lower number of repetitions is identified, and this result is considered for higher repetitions (e.g. if the test

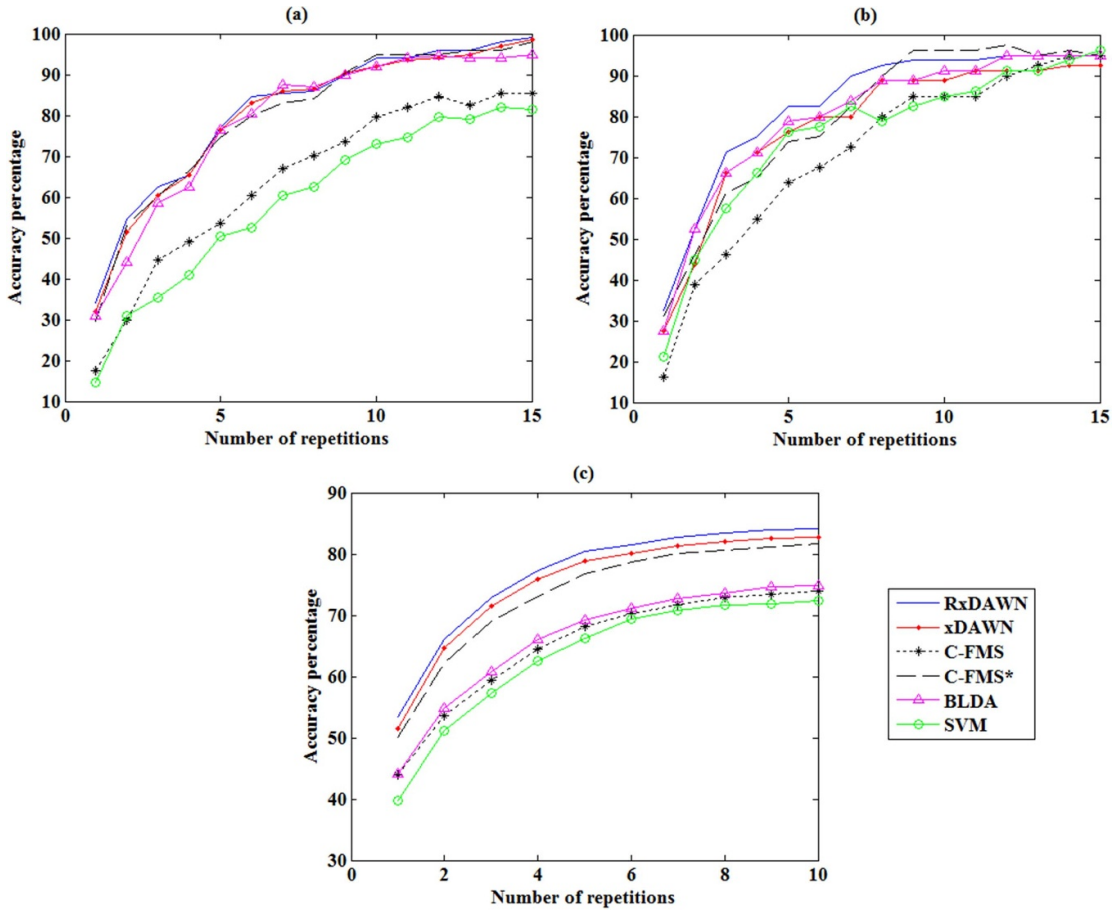

Figure 14. Averaged accuracy results of competing methods for character or object detection across all subjects within each dataset and various repetitions. Data from (a) BCI Competition III-II, (b) BNCI Horizon 2020, and (c) BCIAUT-P300.

data of a session consists of only six repetitions and the maximum result of these six repetitions is 70%, then this 70% result is considered for k_r =7, 8, 9, and 10). In the test phase using the RSVP dataset, as well as in P300 detection experiments with other datasets, the classifier output is obtained for all data samples, and data with higher scores are deemed to contain the P300 signal.

The evaluation of RxDAWN and its competitors relies on robust metrics. This involves calculating the accuracy of character or object detection for each subject across different repetitions. Subsequently, the average results for all subjects within each dataset and various repetitions are reported for each method. Additionally, statistical group tests are performed for all subjects within each dataset. To achieve this, the results from all subjects and repetitions are averaged, and their mean and standard deviation are reported for each method and dataset. The significance of RxDAWN's results is assessed through paired t-tests, and corresponding p-values are provided.

In the case of the RSVP dataset and P300 detection task in other datasets, the objective is to ascertain whether each post-stimulus test data contains P300 and is related to a target stimulus. To address this, the area under the curve (AUC) is calculated for each subject within each dataset. The average AUC of all subjects is then reported for each dataset. This process involves calculating the classifier score for all test data, constructing the receiver operating characteristic (ROC) curve by adjusting the decision threshold on the classifier output, and subsequently computing the AUC of the ROC.

It is crucial to emphasize that the competitors, whose results are detailed in the subsequent section, used the exact same training and test sets, as well as metrics, as RxDAWN.

4.3.3. Results

Figure 14 depicts the averaged character and object detection rates across all subjects within each dataset using various competing algorithms under different SNRs, represented by varying numbers of repetitions during the test phase. In figure 14(a) (data from BCI Competition III-II dataset), the performance of RxDAWN, xDAWN, C-FMS*, and BLDA is closely matched. However, RxDAWN exhibits superior performance in lower SNRs. All four mentioned methods significantly outperform C-FMS and SVM across all SNRs, with C-FMS showing better performance

Table 2. The grand average of character and object detection results over all subjects and repetitions within different datasets. The performance of competing methods is presented in the following format: {%mean ± standard deviation, p-value}.

Method	BCI Competition III-II	BNCI Horizon 2020	BCIAUT-P300
RxDAWN	81.1 ± 19.2, .	82.7 ± 24.2, .	76.6 ± 15.2, .
xDAWN	80.1 ± 19.8, 0.01	78.0 ± 27.3, 0.01	75.1 ± 16.2, 0.01
C-FMS	64.3 ± 22.0, 0.01	71.2 ± 27.7, 0.01	65.2 ± 19.6, 0.01
C-FMS*	79.8 ± 20.5, 0.03	79.8 ± 24.9, 0.01	73.3 ± 17.9, 0.01
BLDA	78.7 ± 20.6, 0.01	80.0 ± 24.1, 0.01	66.2 ± 20.6, 0.01
SVM	59.1 ± 21.3, 0.01	75.4 ± 26.2, 0.01	63.3 ± 18.5, 0.01

Table 3. AUC percentage of different methods for P300 detection. Average results are reported for all subjects within each specified dataset.

Method	BCI Competition III-II	BNCI Horizon 2020	BCIAUT-P300	RSVP
RxDAWN	81.3	84.0	79.8	94.5
xDAWN	81.2	81.4	79.6	93.7
C-FMS	74.5	79.5	74.7	91.8
C-FMS*	81.0	83.3	78.8	94.3
BLDA	80.4	83.4	74.8	93.8
SVM	72.6	81.0	72.5	82.7

than SVM. Moving to figure 14(b) (data from BNCI Horizon 2020 dataset), RxDAWN again demonstrates the best results in low SNRs, while C-FMS* performs better in higher SNRs. SVM detection rates surpass those of C-FMS, particularly in repetitions fewer than eight, with C-FMS exhibiting the poorest performance. In figure 14(c) (data from BCIAUT-P300 dataset), the detection rates among different methods are more distinct due to the larger size of the third dataset. RxDAWN consistently exhibits the best performance across all SNRs, followed by xDAWN and C-FMS*. The results of these three methods are significantly superior to those of BLDA, C-FMS, and SVM. BLDA ranks fourth, C-FMS fifth, and SVM last in performance.

It is important to note that, despite BLDA exhibiting similar performance to other methods in figure 14(a), it utilizes a high number of recording channels (i.e. data from 64 channels). In contrast, methods based on spatial filtering only utilize a few channels. This dimension reduction property of spatial filtering can significantly reduce the computational burden of BCI systems.

Analyzing all three plots in figure 14, it becomes evident that the performance of all methods improves with increasing SNR. Furthermore, it is observed that the performance of C-FMS can notably improve by increasing the number of spatial filters used in C-FMS*. Again, this is attributed to the fact that two dimensions cannot fully span the signal subspace, necessitating more spatial filters for this purpose.

Table 2 presents the grand average of character and object detection results over all subjects and repetitions within each dataset. According to the group statistical tests, for all datasets, RxDAWN demonstrates superior performance compared to other methods at a significance level of $P = 0.05$. For BCI Competition III-II and BCIAUT-P300 datasets, the following best-performing algorithms are xDAWN, C-FMS*, BLDA, C-FMS, and SVM. The order for the BNCI Horizon 2020 dataset is BLDA, C-FMS*, xDAWN, SVM, and C-FMS.

Table 3 reports the AUC results of RxDAWN and its competitors for the P300 detection task over different datasets. As can be seen, for all datasets, RxDAWN has the best performance compared to the other methods. The next best results over BCI Competition III-II and BCIAUT-P300 datasets belong to xDAWN, while BLDA has the next best performance over the BNCI Horizon 2020 dataset, and C-FMS* over the RSVP dataset. Again, it should be noted that although BLDA demonstrates close performance to other methods, it requires all recording channels. However, methods based on spatial filtering only use a few channels, leading to dimension reduction and consequently lowering the computational burden of the BCI system.

To compare the performance of RxDAWN with other powerful methods in the literature, we evaluated our method on the BCI Competition III-II dataset alongside the competition winner (for results, refer to www.bbci.de/competition/iii/results/) and two deep neural network-based methods. The first deep structure is a CNN proposed by Cecotti *et al* [37], while the second one is the 3D-CNN network [25], both customized to detect P300 signals with high accuracy. Table 4 outlines the results of competing methods in 5 and 15 repetitions, noting that the RxDAWN results are the best achieved by different settings. RxDAWN exhibits exemplary performance in 15 repetitions, achieving a very high accuracy of 99% for both SA and SB. For five repetitions, however, RxDAWN is the second-best algorithm in comparison to 3D-CNN, which performs slightly better.

Table 4. The accuracy percentage of the competing methods from the literature over dataset II of BCI Competition III for SA and SB in 5 and 15 repetitions.

	$k_r = 5$			$k_r = 15$		
Method	SA	SB	Avg.	SA	SB	Avg.
Competition winner	72	75	73.5	97	96	96.5
CNN	63	79	71	97	95	96
3D-CNN	74	86	80	96	98	97
RxDAWN	74	85	79.5	99	99	99

Table 5. The mean AUC percentage of RxDAWN and its competing methods from literature for RSVP dataset.

	AUC	
Method	Group A	Group B
EEGNet	92.14	93.19
Improved EEGNet	92.27	93.32
CNN	84.42	85.69
RxDAWN	93.87	95.19

Furthermore, table 5 reports the AUC results of RxDAWN and its competitors from the literature (the well-known EEGNet [27], CNN [37], and improved EEGNet [28]) on the RSVP dataset (all results are from [28]). Note that RxDAWN uses the exact same recording channels (i.e. 1 to 32, 34 to 42, and 44 to 64) referred to in [28]. Based on the findings, it is evident that RxDAWN outperforms the three deep structures, underscoring RxDAWN as a powerful method applicable to both overt and covert paradigms for P300 detection.

5. Discussion

Up to now, many studies have been carried out to design and improve P300-based BCIs. These systems are mostly based on visual P300 and require visual stimuli [6]. These stimuli cause inevitable VEPs in the brain occipital regions which are observable in both target and non-target EEG trials [7]. Despite a large number of studies in the field, the effects of VEPs on the performance of P300-based BCIs have not attracted enough attention. Our study suggests that VEPs should be taken seriously while designing visual P300-based BCIs as they decrease the overall performance of these systems.

When discussing P300 signals, two subcomponents, p3a and p3b, are generally considered [5]. However, in visual P300-based BCIs, VEPs, a sustained and semi-periodic signal, should also be taken into account. Although these potentials are most observable in the brain occipital regions [7], they are transmitted to other scalp regions through volume conduction. Consequently, EEG recordings of any type of visual P300-based BCIs generally have three responses: (1) p3a, observable in both target and non-target post-stimuli recordings, with higher amplitude for target stimuli, (2) p3b, only observable in target trials, and (3) VEPs, observable in both target and non-target trials. VEPs and p3a are both exogenous and mostly induced by phase reset of ongoing brain oscillations, unlike p3b, an endogenous component mostly induced through the additivity mechanism (i.e. adding an ERP to the ongoing brain oscillations) [38].

Some P300-based BCIs are designed based on VEPs (also known as steady state VEPs (SSVEPs)) [39, 40]. In these systems, several sources of stimuli are presented to the subject, and each of them flashes with a specific frequency. The user focuses on the desired target source (which is related to a specific command) causing the brain waves to fluctuate at the same frequency as the source. Therefore, the intended source can be identified in correspondence with the frequency at which the PSD of EEG signals peaks. VEPs-based BCIs are faster than P300-based ones. However, they can generate a limited number of commands at a time compared to P300-based BCIs [41] (for example, in the RCP paradigm in figure 1, the P300 speller can generate 36 commands).

In [42] authors have proposed a creative P300-speller in which not only did'nt they treat SSVEPs (or equally VEPs) as intruders, but also benefited from their phase to improve the classification rate of target sequences. However, this technique required a special paradigm in which characters were displayed on a circular shape and it can not be used for other paradigms such as RCP. Although by using the phase information of SSVEPs the performance of P300-based BCIs can be improved, the results of our study shows that suppressing these potentials will also improve classification rates. Therefore a possible approach is to integrate the two techniques into a two-blocks method to further increase the classification rate.

It is understood that VEPs are more pronounced for target data compared to non-target data in paradigms based on overt attention (such as RCP), and overt paradigms also perform better than covert ones [43]. However, Arico *et al* [44] have shown that the main reason for this performance gap is the lower temporal stability of the P300 evoked potential in covert attention modalities, and not the stronger VEPs for target data. Their research suggests that when compensating for the latency jitter offline, the difference in accuracy between overt and covert paradigms is not significant. Our results for RSVP data are in line with these findings and indicate that RxDAWN can be an effective tool for both overt and covert attention modalities. This is important since, in severe cases of disabilities, some BCI end users may be completely unable to move their eyes.

To mitigate the negative impact of VEPs on visual P300-based BCIs, it is necessary to have a plan in place. One option is to apply a temporal notch filter with a stop-band around the frequency of the visual stimuli. However, this approach may not be effective as VEPs are not pure monotone signals and involve a wider range of frequency components. Moreover, if the stop-band is widened, signal loss can occur since the frequency content of VEPs overlaps with those of P300. An alternative method for suppressing VEPs is spatial filtering. Rivet *et al* [15] developed xDAWN to estimate a subspace in which P300 signals are enhanced. They have found that despite enhancing P300 signals in the obtained subspace, a strong periodic component contributing to VEPs is also present. In this study, we have proposed RxDAWN, an improved version of the xDAWN spatial filter, which can enhance P300 signals and mitigate VEPs simultaneously.

The results of our study confirm the effectiveness of RxDAWN to improve visual P300-based BCIs. However, the RxDAWN algorithm has some limitations. First, based on figure 5, we know that VEPs emerge with delay in the recording electrodes far from occipital regions. This implies that the sensors (electrodes) record a convolutive mixture of different sources rather than their linear instantaneous mixture. RxDAWN (similar to xDAWN) does not benefit from this extra information and this is why in figure 8 for $\alpha = 1$ weight distributions are localized. The second limitation of RxDAWN is that it considers a deterministic response for P300 after each stimulus and estimates a single waveform for P300. Therefore, RxDAWN is not directly applicable to the studies in which the variations of P300 parameters (e.g. amplitude, width, delay) in consecutive trials are of interest (for example studies to determine brain fatigue [45]). However, even in those studies, RxDAWN can be used as a preprocessing stage to enhance the P300 responses.

6. Conclusion

In this article, we investigated the effects of periodic visual stimuli and VEPs on the performance of visual P300-based BCIs. Through temporal, spectral, and spatial analysis of recorded EEG signals, we demonstrated that VEPs contaminate P300 signals and decrease the overall performance of BCIs. We suggested that researchers must consider VEPs as a serious disturbance while designing visual P300-based BCIs and plan a strategy to mitigate them.

Furthermore, we developed RxDAWN, a regularized version of the xDAWN spatial filter, to mitigate VEPs and improve the accuracy of P300-based BCIs. When applied to four publicly available P300 datasets, RxDAWN effectively suppressed VEPs and improved classification rates. RxDAWN outperformed xDAWN, C-FMS, BLDA, SVM, and several powerful deep structures from the literature.

A promising line of future studies involves considering a model based on the convolutive mixture of different sources for the recorded VEPs in different channels, and attempting to suppress them in the time, frequency, or time-frequency domain [46–48]. Since VEPs have semi-periodic nature, another interesting research direction can be adopting a multi-channel Kalman or particle filter to track and suppress these VEPs [49]. One may also incorporate spatial correlation between EEG channels to improve the performance of the filter [17]. There are also some methods in the literature that exploit the quasi-periodicity of signals for source separation which might be effective for VEP cancelation [50, 51].

Data availability statement

The data that support the findings of this study are openly available at the following URLs/DOIs: www.bnci-horizon-2020.eu/database/data-sets, www.bbci.de/competition/iii, www.kaggle.com/datasets/disbeat/bciaut-p300, and http://bci.med.tsinghua.edu.cn/download.html.

Conflict of interest

This research received no specific grant from any funding agency in the public, commercial, or not-for-profit sectors. No potential conflict of interest was reported by the authors.

ORCID iDs

Ali Mobaien https://orcid.org/0000-0003-1874-4289
Reza Boostani https://orcid.org/0000-0003-0055-4452

References

[1] Boostani R and Moradi M H 2004 A new approach in the BCI research based on fractal dimension as feature and Adaboost as classifier *J. Neural Eng.* **1** 212

[2] Boostani R, Graimann B, Moradi M H and Pfurtscheller G 2007 A comparison approach toward finding the best feature and classifier in cue-based BCI *Med. Biol. Eng. Comput.* **45** 403–12

[3] Marcuse L V, Fields M C and Yoo J Y J 2015 *Rowan's Primer of EEG E-Book* (Elsevier Health Sciences)

[4] Philip J T and George S T 2020 Visual P300 mind-speller brain-computer interfaces: a walk through the recent developments with special focus on classification algorithms *Clin. EEG Neurosci.* **51** 19–33

[5] Polich J 2007 Updating P300: an integrative theory of P3a and P3b *Clin. Neurophysiol.* **118** 2128–48

[6] Farwell L A and Donchin E 1988 Talking off the top of your head: toward a mental prosthesis utilizing event-related brain potentials *Electroencephalogr. Clin. Neurophysiol.* **70** 510–23

[7] Creel D J 2019 Visually evoked potentials *Clinical Neurophysiology: Basis and Technical Aspects* (*Handbook of Clinical Neurology* vol 160) ed K H Levin and P Chauvel (Elsevier) ch 34, pp 501–22

[8] Townsend G, LaPallo B K, Boulay C B, Krusienski D J, Frye G, Hauser C, Schwartz N E, Vaughan T M, Wolpaw J R and Sellers E W 2010 A novel P300-based brain–computer interface stimulus presentation paradigm: moving beyond rows and columns *Clin. Neurophysiol.* **121** 1109–20

[9] Fazel-Rezai R and Abhari K 2009 A region-based P300 speller for brain-computer interface *Can. J. Electr. Comput. Eng.* **34** 81–85

[10] Mobaien A, Boostani R, Mohammadi M and Sanei S 2023 ERP detection based on smoothness priors *IEEE Trans. Biomed. Eng.* **70** 867–76

[11] Hoffmann U, Vesin J-M and Ebrahimi T 2006 Spatial filters for the classification of event-related potentials *European Symp. on Artificial Neural Networks (ESANN 2006)*

[12] Fattahi D, Nasihatkon B and Boostani R 2013 A general framework to estimate spatial and spatio-spectral filters for EEG signal classification *Neurocomputing* **119** 165–74

[13] Alimardani F, Boostani R and Blankertz B 2017 Weighted spatial based geometric scheme as an efficient algorithm for analyzing single-trial EEGs to improve cue-based BCI classification *Neural Netw.* **92** 69–76

[14] Xu N, Gao X, Hong B, Miao X, Gao S and Yang F 2004 BCI competition 2003-data set IIb: enhancing P300 wave detection using ICA-based subspace projections for BCI applications *IEEE Trans. Biomed. Eng.* **51** 1067–72

[15] Rivet B, Souloumiac A, Attina V and Gibert G 2009 xDAWN algorithm to enhance evoked potentials: application to brain–computer interface *IEEE Trans. Biomed. Eng.* **56** 2035–43

[16] Campos E, Hazlett C, Tan P, Truong H, Loo S, DiStefano C, Jeste S and Şentürk D 2020 Principle ERP reduction and analysis: estimating and using principle ERP waveforms underlying ERPs across tasks, subjects and electrodes *NeuroImage* **212** 116630

[17] Monajemi S, Jarchi D, Ong S-H and Sanei S 2017 Cooperative particle filtering for tracking ERP subcomponents from multichannel EEG *Entropy* **19** 199

[18] Yang C, Zhang H, Zhang S, Han X, Gao S and Gao X 2019 The spatio-temporal equalization for evoked or event-related potential detection in multichannel EEG data *IEEE Trans. Biomed. Eng.* **67** 2397–414

[19] Kotas M P, Piela M and Contreras-Ortiz S H 2022 Modified spatio-temporal matched filtering for brain responses classification *IEEE Trans. Hum.-Mach. Syst.* **52** 677–86

[20] Blanco-Díaz C, Guerrero-Méndez C and Ruiz-Olaya A 2023 Enhancing P300 detection using a band-selective filter bank for a visual P300 speller *IRBM* **44** 100751

[21] Aghili S N, Kilani S, Khushaba R N and Rouhani E 2023 A spatial-temporal linear feature learning algorithm for P300-based brain-computer interfaces *Heliyon* **9** E15380

[22] Hoffmann U, Vesin J-M, Ebrahimi T and Diserens K 2008 An efficient P300-based brain–computer interface for disabled subjects *J. Neurosci. Methods* **167** 115–25

[23] Salvaris M and Sepulveda F 2009 Wavelets and ensemble of FLDs for P300 classification *2009 4th Int. IEEE/EMBS Conf. on Neural Engineering* (IEEE) pp 339–42

[24] Rakotomamonjy A and Guigue V 2008 BCI competition III: dataset II-ensemble of SVMs for BCI P300 speller *IEEE Trans. Biomed. Eng.* **55** 1147–54

[25] Oralhan Z 2020 3D input convolutional neural networks for P300 signal detection *IEEE Access* **8** 19521–9

[26] Zhang Z, Yu X, Rong X and Iwata M 2021 Spatial-temporal neural network for P300 detection *IEEE Access* **9** 163441–55

[27] Lawhern V J, Solon A J, Waytowich N R, Gordon S M, Hung C P and Lance B J 2018 EEGNet: a compact convolutional neural network for EEG-based brain–computer interfaces *J. Neural Eng.* **15** 056013

[28] Zhang H, Wang Z, Yu Y, Yin H, Chen C and Wang H 2022 An improved EEGNet for single-trial EEG classification in rapid serial visual presentation task *Brain Sci. Adv.* **8** 111–26

[29] Wang Z, Chen C, Li J, Wan F, Sun Y and Wang H 2023 ST-CapsNet: linking spatial and temporal attention with capsule network for P300 detection improvement *IEEE Trans. Neural Syst. Rehabil. Eng.* **31** 991–1000

[30] Du P, Li P, Cheng L, Li X and Su J 2023 Single-trial P300 classification algorithm based on centralized multi-person data fusion CNN *Front. Neurosci.* **17** 1132290

[31] Sandra R, Christian J and Marco C 2012 Designing spatial filters based on neuroscience theories to improve error-related potential classification *2012 IEEE Int. Workshop on Machine Learning for Signal Processing* (IEEE) pp 1–6

[32] Pires G, Nunes U and Castelo-Branco M 2011 Statistical spatial filtering for a P300-based BCI: tests in able-bodied and patients with cerebral palsy and amyotrophic lateral sclerosis *J. Neurosci. Methods* **195** 270–81

[33] Blankertz B, Muller K-R, Krusienski D J, Schalk G, Wolpaw J R, Schlogl A, Pfurtscheller G, Millan J R, Schroder M and Birbaumer N 2006 The BCI competition III: validating alternative approaches to actual BCI problems *EEE Trans. Neural Syst. Rehabil. Eng.* **14** 153–9

[34] Guger C, Daban S, Sellers E, Holzner C, Krausz G, Carabalona R, Gramatica F and Edlinger G 2009 How many people are able to control a P300-based brain–computer interface (BCI)? *Neurosci. Lett.* **462** 94–98

[35] Simões M *et al* 2020 BCIAUT-P300: a multi-session and multi-subject benchmark dataset on autism for P300-based brain-computer-interfaces *Front. Neurosci.* **14** 568104

[36] Zhang S, Wang Y, Zhang L and Gao X 2020 A benchmark dataset for RSVP-based brain–computer interfaces *Front. Neurosci.* **14** 568000

[37] Cecotti H and Graser A 2010 Convolutional neural networks for P300 detection with application to brain-computer interfaces *IEEE Trans. Pattern Anal. Mach. Intell.* **33** 433–45

[38] Cho H, Schalk G, Adamek M, Moheimanian L, Coon W G, Jun S C, Wolpaw J R and Brunner P 2021 Revealing the physiological origin of event-related potentials using electrocorticography in humans *bioRxiv Preprint* (https://doi.org/10.1101/2021.02.12.430921) (posted online 14 February 2021)

[39] Nakanishi M, Wang Y, Wang Y-T, Mitsukura Y and Jung T-P 2014 A high-speed brain speller using steady-state visual evoked potentials *Int. J. Neural Syst.* **24** 1450019

[40] Li M, He D, Li C and Qi S 2021 Brain–computer interface speller based on steady-state visual evoked potential: a review focusing on the stimulus paradigm and performance *Brain Sci.* **11** 450

[41] Zhao J, Li W and Li M 2015 Comparative study of SSVEP- and P300-based models for the telepresence control of humanoid robots *PLoS One* **10** 1–18
[42] Pires G, Yasemin M and Nunes U J 2019 Naturally embedded SSVEP phase tagging in a P300-based BCI: LSC-4Q speller *2019 IEEE Int. Conf. on Systems, Man and Cybernetics (SMC)* (IEEE) pp 2748–53
[43] Treder M S and Blankertz B 2010 (c)overt attention and visual speller design in an ERP-based brain-computer interface *Behav. Brain Funct.* **6** 1–13
[44] Aricò P, Aloise F, Schettini F, Salinari S, Mattia D and Cincotti F 2014 Influence of P300 latency jitter on event related potential-based brain–computer interface performance *J. Neural Eng.* **11** 035008
[45] Jarchi D, Sanei S, Mohseni H R and Lorist M M 2011 Coupled particle filtering: a new approach for P300-based analysis of mental fatigue *Biomed. Signal Process. Control* **6** 175–85
[46] Thi H-L N and Jutten C 1995 Blind source separation for convolutive mixtures *Signal Process.* **45** 209–29
[47] Wu H 1999 Simultaneous diagonalization in the frequency domain (SDIF) for source separation *Proc. 1st Int. Workshop on Independent Component Analysis and Signal Separation, (Aussois, France)*
[48] Rickard S 2001 Real-time time-frequency based blind source separation *Proc. Int. Workshop on Independent Component Analysis and Blind Source Separation, (San Diego, USA)* pp 651–6
[49] Sameni R, Shamsollahi M B, Jutten C and Babaie-Zade M 2005 Filtering noisy ECG signals using the extended Kalman filter based on a modified dynamic ECG model *Computers in Cardiology* (IEEE) pp 1017–20
[50] Sameni R, Jutten C and Shamsollahi M B 2008 Multichannel electrocardiogram decomposition using periodic component analysis *IEEE Trans. Biomed. Eng.* **55** 1935–40
[51] Tsalaile T, Sameni R, Sanei S, Jutten C and Chambers J 2008 Sequential blind source extraction for quasi-periodic signals with time-varying period *IEEE Trans. Biomed. Eng.* **56** 646–55